Available online at www.sciencedirect.com
SCIENCE DIRECT®
Acta Materialia 52 (2004) 3069–3074
Acta MATERIALIA
www.actamat-journals.com

# Spinodal decomposition in a film with periodically distributed interfacial dislocations

S.Y. Hu *, L.Q. Chen

*Department of Materials Science and Engineering, The Pennsylvania State University, 305 Steidle Building, State College, University Park, PA 16802, USA*

Received 19 February 2004; received in revised form 19 February 2004; accepted 6 March 2004
Available online 20 April 2004

**Abstract**

Phase field approach is applied to modeling the spinodal decomposition process in a thin film with periodically distributed arrays of interfacial dislocations. The elastic stress field in the simultaneous presence of interfacial dislocations, substrate constraint, and compositional strains is obtained by solving the mechanical equilibrium equations using an iteration method. It is shown that the periodic stress field associated with the array of interfacial dislocations leads to a directional phase separation and the formation of ordered mesoscale microstructures. It is demonstrated that when the periodicity of the dislocation is small, the wavelength of the ordered microstructure tends to be the same periodicity as the dislocation array. The results have important practical implications that an ordered nanostructures could be produced by controlling the interfacial dislocation distribution.


*Keywords:* Spinodal decomposition; Interfacial dislocation; Thin film; Phase field models

## 1. Introduction

The translational symmetry in bulk materials is broken due to the presence of a surface and an interface in a thin film on a substrate [1]. As a result, the kinetics of phase transition in a film may differ dramatically from that in bulk materials. For example, quasi-two dimensional diffusion may occur in a very thin film, and results in the formation of cylindrical particles perpendicular to the surface during spinodal decomposition. For a thick film, the stress relaxation at surface or stress gradient along the film thickness causes an inhomogeneous decomposition rate and the development of alternating layers of the phases lying parallel to the surface [2–4]. Experiments demonstrated that a regular network of pure edge-type dislocations with a spacing of several nanometers could be formed directly at the heterointerface, which has extremely large lattice mismatches between the film and substrate [5–7]. The effects of dislocations on spinodal decomposition [8] and morphological instability [9] were studied. Like a surface, interfacial dislocations and a strained or patterned substrate break the translational symmetry in the film plane, which can be used to control the wave length of spinodal decomposition and thus the resulting nanostructures [1,7,10–14]. Romanov et al. [12] investigated the possibility of using such dislocation arrays to control the nucleation of self-assembled quantum dots. Johnson et al. [1,10,11] performed two-dimensional simulations of phase decomposition in a film on a patterned substrate. Greaney et al. [14] studied the effect of a rigid, periodically strained substrate on spinodal decomposition in a film. A linear stability analysis [14] showed that a film will undergo spinodal decomposition with the dominant wavelength determined by the periodicity of the substrate strain. The purpose of the present work is to develop a three-dimensional (3D) phase field model for simulating the spinodal decomposition in a film with periodically distributed interfacial dislocations and subject to an elastically substrate constraint. The iteration

* Corresponding author. Tel.: +1-814-865-0389; fax: +1-814-865-2917.
*E-mail address:* sxh61@psu.edu (S.Y. Hu).

1359-6454/$30.00 © 2004 Acta Materialia Inc. Published by Elsevier Ltd. All rights reserved.
doi:10.1016/j.actamat.2004.03.029

method proposed for solving mechanical equilibrium equations in elastically inhomogeneous bulk solids [15] is extended to thin films in the simultaneous presence of dislocations, compositional strains, and a substrate constraint. Although the surface instabilities of the film can also be taken into account, in the present work, we assume that the film has a flat surface. The formation of self-assembled quantum dots due to surface instabilities will be reported in a coming paper.

## 2. Phase-field model

We consider a cubic thin film grown heteroepitaxially on a cubic substrate at high temperature. We assume that a periodically dislocation array is formed at the interface. The Burgers' vectors of dislocations are assumed to be along $\frac{1}{2}[1\,1\,0]$ and $\frac{1}{2}[\bar{1}\,1\,0]$, respectively. For simplicity, we assume the film is a binary solid solution, which is unstable with respect to spinodal decomposition at the temperature of interest. In the phase-field framework, the composition $c(\boldsymbol{x},t)$, which represents the mole or atom fraction at position $x$ and time $t$, is chosen as the phase variable. If we ignore the microstructural evolution of the substrate and the dislocation core energy, then the total energy of the system includes the chemical free energy, gradient energy due to composition inhomogeneity, and elastic energy

$$E=\int_v [f(c(\boldsymbol{x},t))+\frac{\alpha^2}{2}(\nabla c(\boldsymbol{x},t))^2 + \frac{1}{2}\lambda_{ijkl}(\boldsymbol{x},t)\varepsilon_{ij}(\boldsymbol{x},t)\varepsilon_{kl}(\boldsymbol{x},t)]d^3x, \quad (1)$$

where $f(c)$ is the chemical free energy density, $\alpha$ is the gradient energy coefficient. The third term in (1) is the elastic energy density. $\lambda_{ijkl}(x,t)$ is the elastic modulus tensor, which is, in general, spatially dependent. For evolving microstructures, it might be time dependent. $\varepsilon_{ij}(x,t)$ is the elastic strain tensor, which is obtained by solving the mechanical equilibrium equations.

### 2.1. Chemical free energy

The chemical free energy density, $f(c)$, is arbitrarily chosen as a double well function which has minima at equilibrium compositions of 0.053, and 0.947 as follows:

$$f(c)=f_0(-(c-0.5)^2+2.5(c-0.5)^4), \quad (2)$$

where $f_0$ is a scaled constant.

### 2.2. Elastic energy

We assume that the variation of stress-free lattice parameter, $a$, with composition obeys Vegard's law, the local stress-free strain tensor or eigenstrain tensor caused by compositional inhomogeneity is given by

$$\varepsilon^c_{ij}(\boldsymbol{x},c(\boldsymbol{x},\boldsymbol{t}))=\varepsilon_0\delta c(\boldsymbol{x},\boldsymbol{t})\delta_{ij}, \quad (3)$$

where $\varepsilon_0=(1/a)(\mathrm{d}a/\mathrm{d}c)$ is the composition expansion coefficient of lattice parameter, $\delta c(\boldsymbol{x},t)=c(\boldsymbol{x},t)-c_0$ with $c_0$ being the overall composition of the solid solution, and $\delta_{ij}$ is the Kronecker-delta function.

Dislocations are viewed as one kind of lattice distortions. The eigenstrain tensor related to a dislocation loop on slip plane $p$ with a Burgers vector $\mathbf{b}$, can be described as [16–19]

$$\varepsilon^{\mathrm{dis0}}_{ij}(\boldsymbol{x})=\frac{1}{2d_0}(b(i)n(j)+b(j)n(i))\delta(\boldsymbol{x}-\boldsymbol{x}_0), \quad (4)$$

where $\boldsymbol{n}$ is the unit vector normal to the slip plane, $d_0$ is the interplanar distance of the slip planes. $\delta(\boldsymbol{x}-\boldsymbol{x}_0)$ is the Dirac delta function and $\boldsymbol{x}_0$ is a point inside the dislocation loop on the slip plane. For a spatial distribution of many dislocation loops, the total eigenstrain $\varepsilon^{\mathrm{dis}}_{ij}(\boldsymbol{x})$ can be obtained by adding the eigenstrain tensor of individual dislocation loops. Hence, the total eigenstrain tensor associated with the composition inhomogeneity and dislocations can be written as

$$\varepsilon^0_{ij}(\boldsymbol{x})=\varepsilon^c_{ij}(\boldsymbol{x})+\varepsilon^{\mathrm{dis}}_{ij}(\boldsymbol{x}). \quad (5)$$

In a bulk system with periodic boundary conditions, several methods were developed for finding the elastic solution in an elastically inhomogeneous system [15,20–22]. In the present work, the iteration method in [15] is extended to thin films. To do this, we artificially add a gas phase above the film as shown in Fig. 1. By applying periodic boundary conditions to the film system in $x$-, $y$- and $z$-directions, a 3D bulk system is constructed. The iteration method can be directly employed to find the elastic solution in the film by assigning a zero elastic constant in the gas phase. The eigenstrain and elastic modulus tensors are defined as

$$\varepsilon^0_{ij}(\boldsymbol{x})=\begin{cases}\varepsilon^{\mathrm{dis}}_{ij}(\boldsymbol{x}) & \text{in the gas phase,}\\ \varepsilon^c_{ij}(\boldsymbol{x})+\varepsilon^{\mathrm{dis}}_{ij}(\boldsymbol{x}) & \text{in film and substrate,}\end{cases} \quad (6)$$

and

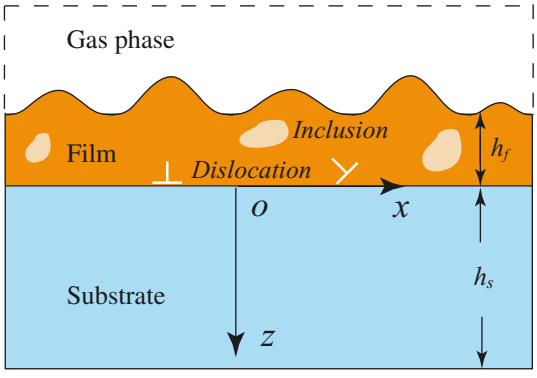


Fig. 1. Schematic drawing of an elastically inhomogeneous system.

$$\lambda_{ijkl}(\boldsymbol{x}) = \lambda^0_{ijkl} + \lambda'_{ijkl}(\boldsymbol{x}) = \begin{cases} 0.0 & \text{in the gas phase,} \\ \lambda^0_{ijkl} + \lambda'_{ijkl}(\boldsymbol{x}) & \text{in film and substrate,} \end{cases} \quad (7)$$

where $\lambda^0_{ijkl}(\boldsymbol{x})$ is the elastic constant of one of the phases in the system, $\lambda'_{ijkl}(\boldsymbol{x})$ is the change in elastic constants with respect to $\lambda^0_{ijkl}(\boldsymbol{x})$. Notice that the elastic constant is zero in the gas phase, so all stress components are zero in the gas phase. From the continuity of stresses at the interface between the gas phase and the solid phase, the elastic solution obtained satisfies the stress-free boundary conditions at the surface of the film ($z = h_f$), and the bottom of the substrate ($z = h_s$). In the present work, we assume the film and substrate are elastically homogeneous, i.e., $\lambda'_{ijkl}(\boldsymbol{x}) = 0$.

To verify the iteration method in the film system, we consider a single edge dislocation below the surface as shown in Fig. 2, which has analytical solutions [23]. The simulation cell is $512 \times 1 \times 256$, where $h = 40$ and $l = 1$. The dislocation below the surface and its image dislocation in the gas phase form a dislocation loop. The nonzero eigenstrain associated with such a dislocation loop is

$$\varepsilon^{\text{dis}}_{11}(\boldsymbol{x}) = b/d_0\delta(\boldsymbol{x} - \boldsymbol{x}_0), \quad (8)$$

where $b$ is the magnitude of the Burgers vector of the dislocation, $d_0$ is the grid spacing. $\boldsymbol{x}_0$ is the point within the dislocation loop on the slip plane. Distributions of stress components $\sigma_{11}(z)$ and $\sigma_{22}(z)$ along A–A line shown in Fig. 2 are plotted in Fig. 3(a) and (b) for different iteration numbers. The analytical solutions are also included for comparison. It is found that the numerical solution with eight iterations agrees very well with the analytical solution. In the numerical simulation of spinodal decomposition, the elastic solution at time $t$ is used as the zeroth order solution for $t + \Delta t$, and hence, three iterations is sufficient for obtaining the elastic solution.

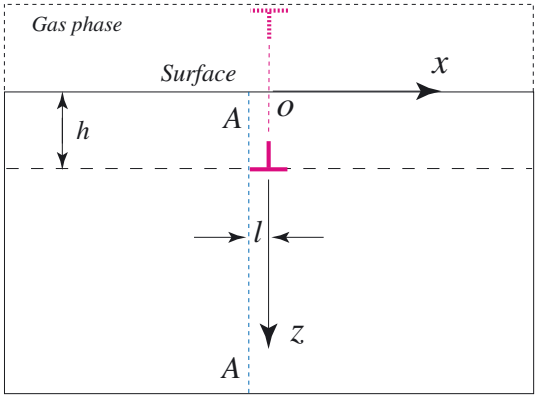


Fig. 2. The image dislocation in the gas phase and the real dislocation below the surface form a dislocation loop.

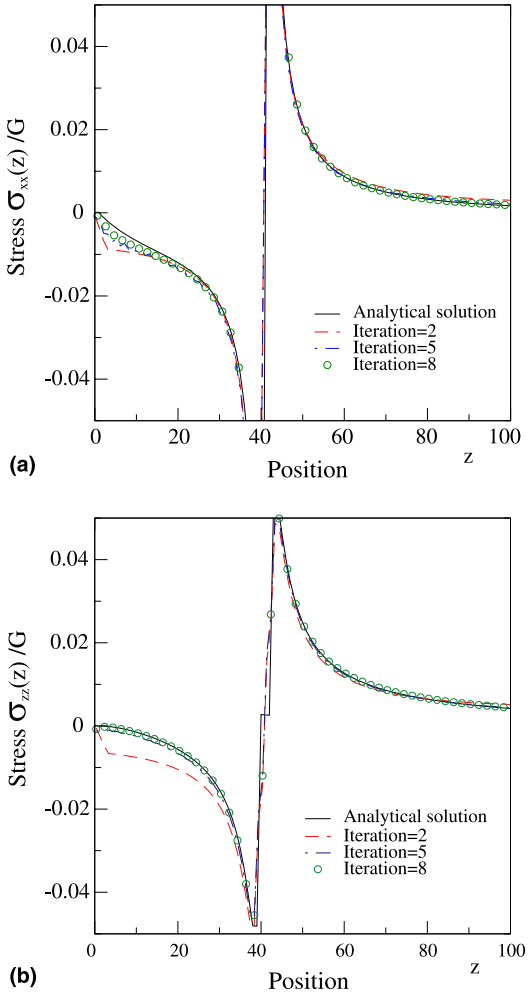


Fig. 3. (a) $\sigma_{xx}(z)/G$ and (b) $\sigma_{zz}(z)/G$ along A–A line shown in Fig. 2.

### 2.3. Evolution equation

Since the composition is a conserved field variable, its evolution is described by the Cahn–Hilliard-type diffusion equation [24]

$$\frac{\partial c(\boldsymbol{x},t)}{\partial t} = \nabla M \nabla \frac{\delta E}{\delta c(\boldsymbol{x},t)} + \xi(\boldsymbol{x},t), \quad (9)$$

where $\delta E/\delta c(\boldsymbol{x},t)$ denotes the variational derivative, the function $\xi(\boldsymbol{x},t)$ is a statistically defined Gaussian white noise source with mean zero

$$\langle \xi(\boldsymbol{x},t) \rangle = 0, \quad (10)$$

where $M$ is chemical mobility. If we assume that the atomic mobilities of species 1 and 2 are equal, the mobility, $M$, is given by

$$M = \frac{Dc(\boldsymbol{x},t)(1 - c(\boldsymbol{x},t))}{k_B T}, \quad (11)$$

where $D$ is the chemical diffusion coefficient, $k_B$ is the Boltzmann constant and $T$ is the absolute temperature.

The variation of the total free energy (1) with respect to composition $c(\boldsymbol{x},t)$ gives

$$\frac{\partial c(\boldsymbol{x},t)}{\partial t} = \nabla\cdot\left[\frac{Dc(\boldsymbol{x},t)(1-c(\boldsymbol{x},t))}{k_{\mathrm{B}}T}\nabla\left(\frac{\partial f(c(\boldsymbol{x},t))}{\partial c(\boldsymbol{x},t)} - \alpha\nabla^2 c(\boldsymbol{x},t) + \mu_{\mathrm{el}}(\boldsymbol{x},t)\right)\right] + \xi(\boldsymbol{x},t), \tag{12}$$

where $\mu_{\mathrm{el}}$ is the elastic potential which is the derivative of the elastic energy with respect to composition.

Using reduced variables we have the dimensionless form of the evolution equation

$$\frac{\partial c(r^*,t^*)}{\partial t^*} = (\nabla^*)^2\left(\frac{\partial f^*(c(r^*,t^*))}{\partial c(r^*,t^*)} - \alpha^*(\nabla^*)^2 c(r^*,t^*) + \mu^*_{\mathrm{el}}(r^*,t^*)\right) + \xi(r^*,t^*), \tag{13}$$

where $\boldsymbol{r}^* = \boldsymbol{x}/d_0$, $t^* = Dtc_0(1-c_0)/d_0^2$, $\nabla^* = d_0\nabla$, $f^* = f/(k_{\mathrm{B}}T)$, $\alpha^* = \alpha/(k_{\mathrm{B}}Td_0^2)$ and $\mu^*_{\mathrm{el}} = \mu_{\mathrm{el}}/(k_{\mathrm{B}}T)$, where $d_0$ is the grid spacing.

In the present work, we ignore the morphological instabilities in the film surface, and assume the composition flux at the surface of the film and interface between the film and the substrate are zero. Therefore, the temporal evolution of the composition field is obtained by solving the Eq. (13) together with the initial conditions and the following boundary conditions

$$\left.\frac{\partial c(\boldsymbol{x},t)}{\partial z}\right|_{z=-h_{\mathrm{f}}} = 0 \quad \text{and} \quad \left.\frac{\partial c(\boldsymbol{x},t)}{\partial z}\right|_{z=0} = 0. \tag{14}$$

To numerically solve this evolution equation, a Fourier-spectral method is used in $x$- and $y$-directions [4,25]. Since the zero-flux boundary conditions at film surface and film/substrate interface cannot be satisfied by a Fourier expansion, a second-order finite difference method with fast Fourier transform (FFT) is used in the $z$-direction.

## 3. Results and discussion

In the simulation, $128\times128\times32$ discrete grid points are used. The thickness of the substrate is $h_{\mathrm{s}} = 18$. In order to study the effect of film thickness on the microstructural pattern, three different film thickness $h_{\mathrm{f}} = 3$, 5 and 9 are considered. The dimensionless grid spacing is chosen to be $\Delta x_1/d_0 = \Delta x_2/d_0 = \Delta x_3/d_0 = 1.0$ and $\Delta t^*$ is chosen to be 0.05. The interfacial energy is assumed to be isotropic, and the dimensionless gradient energy coefficient, $\alpha^*$, is taken to be 0.5. The overall reduced composition used in this study is 0.5 which is inside the spinodal decomposition region. Isotropic elastic constants are assumed for both film and substrate, $C_{11} = 300$, $C_{12} = 100$, $C_{44} = 100$, in the unit of $N_{\mathrm{V}}k_{\mathrm{B}}T$ where $N_{\mathrm{V}}$ is the number of atoms per unit volume. Considering that the linear elasticity theory is only valid outside the dislocation core region, the characteristic length $d_0$ is taken to be $10b$, where $b$ is the magnitude of the Burgers' vector of the dislocation.

In the present work, our main focus is on the effect of nonuniform lattice mismatches at the film/substrate interface on morphological evolution during spinodal decomposition. The nonuniform interface lattice mismatches are related to interfacial dislocations. Assume $nx$ edge dislocations and $ny$ edge dislocations are uniformly distributed in $x$- and $y$-directions, respectively. The nonzero components of the eigenstrain tensor related to such a dislocation distribution can be described as

$$\begin{aligned}\varepsilon^{\mathrm{dis}}_{11}(\boldsymbol{r}) &= \sum_{n_1=1}^{nx}\frac{b}{d_0}\delta\left(x-\left(\frac{128}{nx}-0.5\right)\right),\\ \varepsilon^{\mathrm{dis}}_{22}(\boldsymbol{r}) &= \sum_{n_2=1}^{ny}\frac{b}{d_0}\delta\left(y-\left(\frac{128}{ny}-0.5\right)\right),\\ &\text{if } z < h_{\mathrm{f}}.\end{aligned} \tag{15}$$

First, let us compare the composition evolution in two cases. In case I, the lattice mismatch is uniform, $\varepsilon^{\mathrm{dis}}_{11} = \varepsilon^{\mathrm{dis}}_{22} = 0.00165$. And in case II, the total lattice mismatch is the same as that in case I, but the uniform lattice mismatch is replaced by two dislocations in both $x$- and $y$-directions. The thickness of the film is $3d_0$. We start the simulation with a very small composition fluctuation. Fig. 4 shows the snapshots of composition evolution in the course of spinodal decomposition. The red color denotes solute rich region while white color solvent rich region. It is clearly seen that two interconnected phases gradually formed in case I. Since the film is very thin, and the diffusion fluxes normal to the surface and the interface are zero, diffusion occurs primarily on the plane parallel to the interface. As a result, each phase has a columnar morphology perpendicular

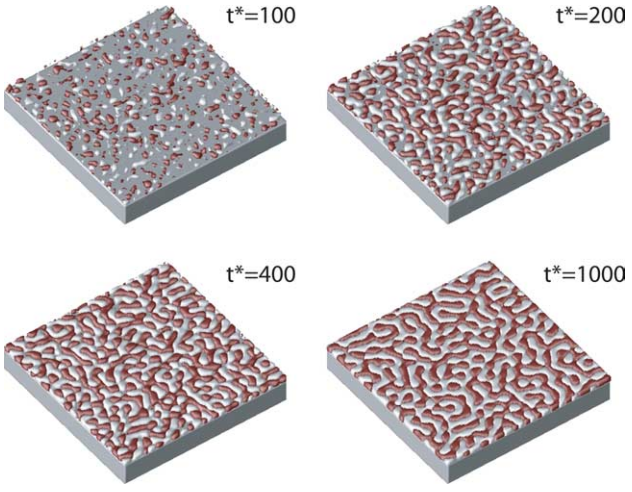


Fig. 4. Temporal morphological evolution during spinodal decomposition in a thin film under a uniform substrate constraint.

to the interface. Our previous results [4] show that as the film thickness increases, the morphology of each phase becomes a 3D network similar to that of bulk materials.

For case II, the interaction between stress fields from interfacial dislocations and compositional strains dominates the spinodal decomposition process and causes a directional spinodal decomposition. Fig. 5 presents the morphological evolution during spinodal decomposition in the film. To see more clearly the composition wave evolution, Fig. 6 plots the temporal composition evolution along A–A line at $z = 2$ shown in Fig. 5. We can see that at the initial stage the local stress results in the formation of composition waves near the dislocation along the direction perpendicular to the dislocation line on the film plane as well as along the thickness direction. The composition wave along thickness is transient. As time increases, such a composition wave disappears. The composition wave along the direction perpendicular to the dislocation line on the film plane propagates directionally as time increases. Finally, a mesoscopically ordered microstructure is formed.

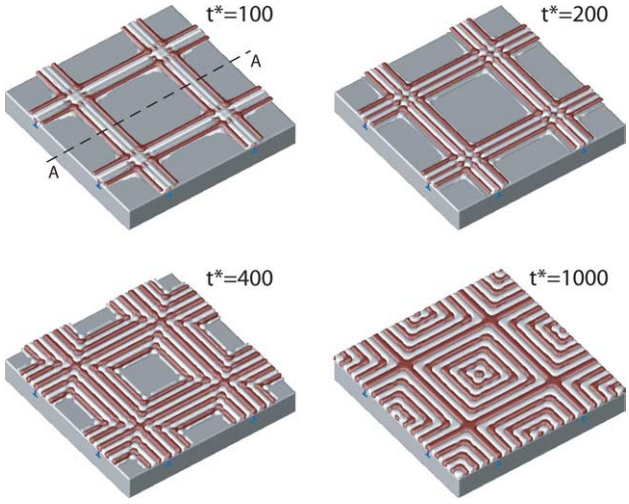


Fig. 5. Temporal morphological evolution during spinodal decomposition in a thin film with two interfacial dislocations in both $x$- and $y$-directions.

To illustrate the effect of the wavelength of dislocation distributions on the microstructure pattern, four different dislocation distributions ($nx = ny = 2$, 4, 8 and 16) are simulated. Fig. 7 presents the microstructure patterns at simulation step $t = 1000$. It can be seen that with the increase of the dislocation density or the decrease of their periodicity, the morphology of two decomposed phases changes dramatically from interconnected to isolated particles. The results demonstrate that a nanostructure can be obtained by decreasing the wavelength of dislocation distributions. Fig. 8 illustrates how the thickness of the film affects the microstructure patterns. The microstructures at simulation step $t = 1000$ are shown for three different simulations corresponding to three different film thickness $h_f = 3$, 5 and 9 for the case with eight dislocations ($nx = ny = 8$). The left figure presents the morphology

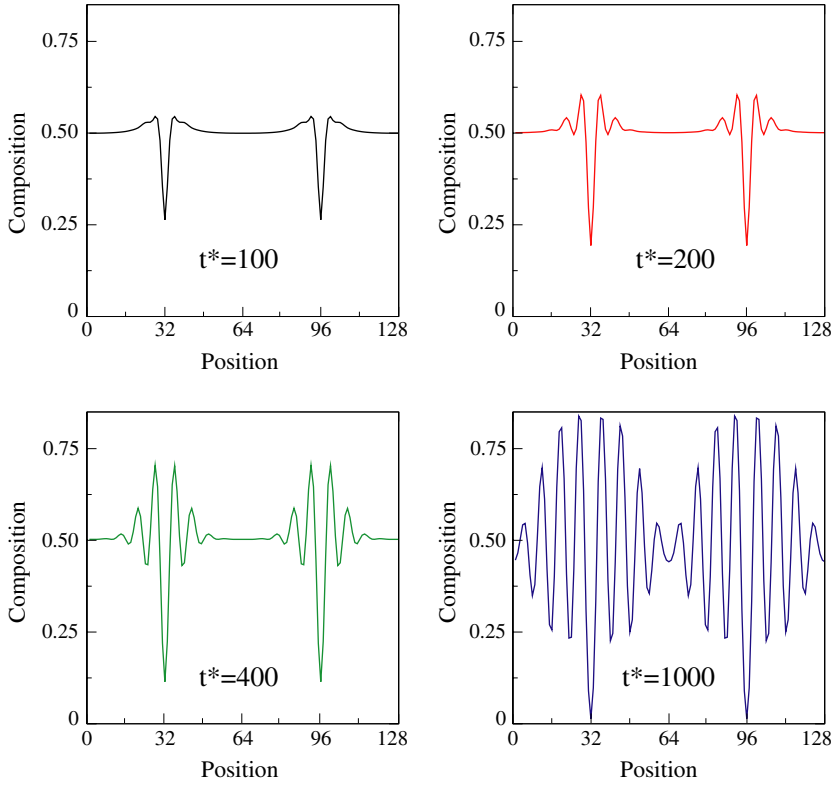


Fig. 6. Composition profile along A–A line shown in Fig. 5 during spinodal decomposition.

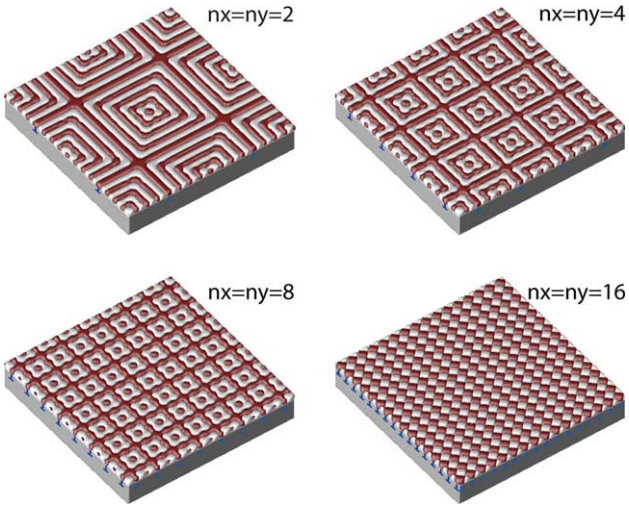


Fig. 7. Microstructural patterns formed during spinodal decomposition with different interfacial dislocation arrays.

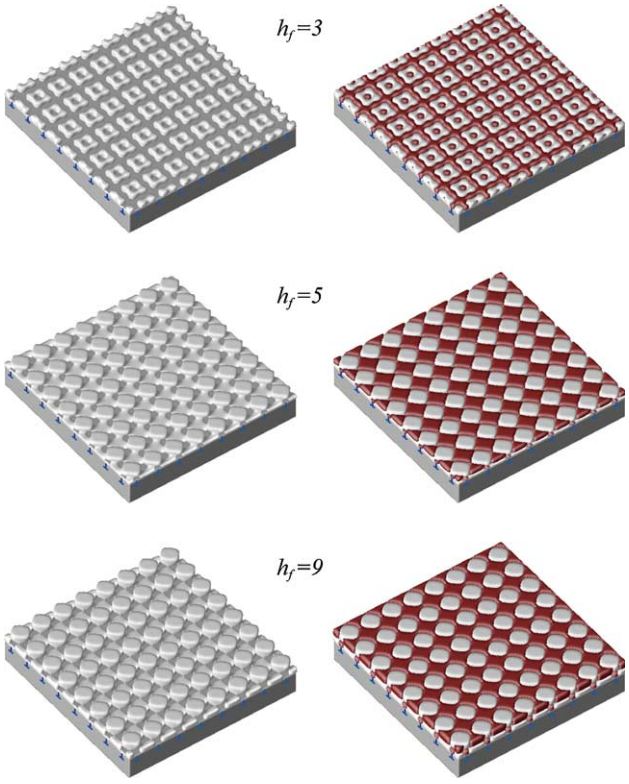


Fig. 8. Effect of film thickness on microstructural patterns with eight interfacial dislocations in both $x$- and $y$-directions.

of the solute rich phase. It is clearly seen that as the thickness increases, the composition wave along the thickness direction starts to form. With sufficient thickness, a microstructure with two alternating layers of the phases is developed. In addition, the morphology of the phases in each layer is different from that in the thin films ($h_f = 3$).

## 4. Conclusion

We developed a phase-field model to simulate the effect of a periodically distribution of interfacial dislocations on spinodal decomposition in an elastically constraint film. The iteration method is shown to be efficient in obtaining the elastic solutions. Simulation results demonstrate that the dislocation stresses induce a directional spinodal decomposition. Periodically distributed interfacial dislocations can be used to create self-assembled nanostructures. The nanostructure can be changed by varying the film thickness and the wavelength of the interfacial dislocation distribution.

## References

[1] Johnson WC, Wise SM. Appl Phys Lett 2002;81:919.
[2] Brown G, Chakrabarti A. Phys Rev A 1992;46:4829.
[3] Puri S, Binder K. J Stat Phys 1994;77:145.
[4] Seol DJ, Hu SY, Li YL, Shen J, Oh KH, Chen LQ. Acta Mater 2003;51:5173.
[5] Chang JCP, Chin TP, Woodall JM. Appl Phys Lett 1996;69:981.
[6] Lee EY, Bhargava S, Chin MA, Narayanamurti V, Pond KJ, Luo K. Appl Phys Lett 1996;69:940.
[7] Brune H, Giovannini M, Bromann K, Kern K. Nature 1998;394:451.
[8] Le'onard F, Desai R. Phys Rev B 1998;58:8277.
[9] Haataja M, Muller J, Rutenberg AD, Grant M. Phys Rev B 2002;65:165414.
[10] Wise SM, Johnson WC. J Appl Phys 2003;94:889.
[11] Leo HP, Johnson WC. Acta Mater 2001;49:1771.
[12] Romanov AE, Petroff PM, Speck JS. Appl Phys Lett 1999;74:2280.
[13] Ipatova IP, Malyshkin VG, Shchukin VA. J Appl Phys 1993;74:7198.
[14] Greaney PA, Clemens BM, Nix WD, Chrzan DC. Appl Phys Lett 2003;83:1364.
[15] Hu SY, Chen LQ. Acta Mater 2001;49:463.
[16] Trial T, Mura T. Micromechanics in solids. Dordrecht: Kluwer Academic; 1982.
[17] Hu SY, Chen LQ. Acta Mater 2001;49:463.
[18] Wang YU, Jin YM, Cuitino AM, Khachaturyan AG. Appl Phys Lett 2001;78:3071.
[19] Rodney D, Bouar YLE, Finel A. Acta Mater 2003;51:17.
[20] Onuki A. J Phys Soc Jpn 1989;58:3065.
[21] Sagui C, Somoza AM, Desai R. Phys Rev E 1994;50:4865.
[22] Wang YU, Jin YM, Khachaturyan AG. Appl Phys Lett 2002;80:4513.
[23] . first ed.,..Indenbom VL, Lothe J, editors. Elastic strain fields and dislocation mobility, vol. 31. North-Holland: Elsevier; 1992.
[24] Cahn JW. Acta Metall 1961;9:795.
[25] Chen LQ, Shen J. Comput Phys Commun 1998;108:147.